Monthly Notices of the ROYAL ASTRONOMICAL SOCIETY

MNRAS **489,** L91–L96 (2019) doi:10.1093/mnrasl/slz133
Advance Access publication 2019 August 29

Multimessenger Bayesian parameter inference of a binary neutron star merger

Michael W. Coughlin [1]★ Tim Dietrich,[2] Ben Margalit[3]† and Brian D. Metzger[4]

[1] *Division of Physics, Math, and Astronomy, California Institute of Technology, Pasadena, CA 91125, USA*
[2] *Nikhef, Science Park 105, NL-1098 XG Amsterdam, the Netherlands*
[3] *Department of Astronomy, University of California, Berkeley, CA 94720, USA*
[4] *Department of Physics and Columbia Astrophysics Laboratory, Columbia University, New York, NY 10027, USA*

Accepted 2019 August 26. Received 2019 August 15; in original form 2019 July 12

ABSTRACT

The combined detection of a binary neutron star merger in both gravitational waves (GWs) and electromagnetic (EM) radiation spanning the entire spectrum – GW170817/AT2017gfo/GRB170817A – marks a breakthrough in the field of multimessenger astronomy. Between the plethora of modelling and observations, the rich synergy that exists among the available data sets creates a unique opportunity to constrain the binary parameters, the equation of state of supranuclear density matter, and the physical processes at work during the kilonova and gamma-ray burst. We report, for the first time, Bayesian parameter estimation combining information from GW170817, AT2017gfo, and GRB170817 to obtain truly multimessenger constraints on the tidal deformability $\tilde{\Lambda} \in [302, 860]$, total binary mass $M \in [2.722, 2.751]\,\mathrm{M}_{\odot}$, the radius of a 1.4 solar mass neutron star $R \in [11.3, 13.5]$ km (with additional 0.2 km systematic uncertainty), and an upper bound on the mass ratio of $q \leq 1.27$, all at 90 per cent confidence. Our joint novel analysis uses new phenomenological descriptions of the dynamical ejecta, debris disc mass, and remnant black hole properties, all derived from a large suite of numerical relativity simulations.

Key words: gravitational waves – methods: statistical.

1 INTRODUCTION

The combined detection of a gravitational wave (GW) event, GW170817 (Abbott et al. 2017a), a gamma-ray burst (GRB) of short duration, GRB170817A (Abbott et al. 2017c) accompanied by a non-thermal afterglow, and thermal emission (kilonova) at optical, near-infrared, and ultraviolet wavelengths, AT2017gfo (e.g. Abbott et al. 2017b; Arcavi et al. 2017; Coulter et al. 2017; Lipunov et al. 2017; Soares-Santos et al. 2017; Tanvir et al. 2017; Valenti et al. 2017), from a binary neutron star (BNS) merger has enabled major leaps forward in several research areas. The latter includes new limits on the equation of state (EOS) of cold matter at supranuclear densities (e.g. Margalit & Metzger 2017; Abbott et al. 2018; Coughlin et al. 2018; De et al. 2018; Radice et al. 2018b). One of the main goals of the nascent field of 'multimessenger astronomy' is to obtain complementary observations of the same object or event. These observations, potentially across a variety of wavelengths and particle types, probe different aspects of the system. In the case of GW170817, GW detectors such as LIGO and Virgo provide a highly accurate measurement of the binary chirp mass $\mathcal{M} = 1.186\,\mathrm{M}_{\odot}$, but leave the mass ratio, q, poorly constrained.

A variety of studies over the last year focused on the properties of this first detection of a BNS system, including detailed analyses of the GW signal by the LVC (e.g. Abbott et al. 2017a, 2018, 2019a,b) and external groups (e.g. Dai, Venumadhav & Zackay 2018; De et al. 2018; Finstad et al. 2018), relying on different parameter estimation techniques and a variety of GW models. Despite this diversity of methods, all of the published works predict small tidal deformabilities, favouring relatively soft EOSs and placing upper limits on the radii of NSs. For this first BNS system the GW analyses broadly agree, and studies indicate that systematic errors are below the statistical errors (Abbott et al. 2019a; Dudi et al. 2018; Samajdar & Dietrich 2018). However, this might not be the case for future GW observations with larger signal-to-noise ratios, thus emphasizing the need for further improvements in the current infrastructure and GW modelling.

Fortunately, deficiencies in the available GW information can sometimes be supplemented with electromagnetic (EM) observations, potentially improving the measurements of key parameters. For instance, the results of numerical relativity (NR) simulations were used to argue against the EOS being too soft, as the mass of the remnant accretion disc and its associated wind ejecta would be

★ E-mail: mcoughli@caltech.edu
† NASA Einstein Fellow.

insufficient to account for the luminosity of the observed kilonova (e.g. Bauswein et al. 2017; Coughlin et al. 2018; Radice et al. 2018a). Combining GW and EM observations thus provides an opportunity to independently constrain the binary parameters, place tighter bounds on the EOS, and obtain a better understanding of the physical processes and outcomes of BNS mergers.

One of the first multimessenger constraints on the tidal deformability and supranuclear EOS was presented in Radice et al. (2018b). Based on NR simulations, the authors proposed that the tidal deformability needs to be $\tilde{\Lambda} \geq 400$ to ensure that a significant fraction of matter was either ejected from the system or contained within a debris disc around the BH remnant to explain the bright EM counterpart. Recently, Radice & Dai (2019) updated this first analysis and obtained constraints on the tidal deformability of $\tilde{\Lambda} \in (323, 776)$ and on the corresponding radius of a $1.4\,\mathrm{M}_{\odot}$ neutron star of $12.2^{+1.0}_{-0.8} \pm 0.2$ km, performing a multimessenger parameter estimation incorporating information from the disc mass (Radice et al. 2018c). Kiuchi et al. (2019) also show that the possibility of higher mass ratio systems argues for an even lower bound, $\tilde{\Lambda} \geq 242$. We note that this bound of $\tilde{\Lambda} \geq 242$ will be perfectly consistent with the 90 per cent confidence interval that we will find in our work considering that only 7 per cent of the data set of Kiuchi et al. (2019) will not fall without our confidence interval.

To the best of our knowledge, Coughlin et al. (2018) presented the first analysis of the light curves and spectra of AT2017gfo, which linked a Bayesian analysis the kilonova properties to the source properties of the binary. We used the kilonova model of Kasen et al. (2017) combined with methods of Gaussian process regression (GPR; Pürrer 2014; Doctor et al. 2017; Coughlin et al. 2018) and related a fraction of the ejected material to dynamical ejecta. Based on the analysis, the tidal deformability was limited to $\tilde{\Lambda} > 197$.

In addition, there have been studies placing limits on the maximum NS mass of a stable TOV star, M_{TOV}. Those studies are orthogonal to the works constraining the tidal deformability since both quantities ($\tilde{\Lambda}$, M_{TOV}) test different parts of the NS EOS. Margalit & Metzger (2017) place a 90 per cent upper limit on the mass of a non-rotating NS of $2.17\,\mathrm{M}_{\odot}$, Rezzolla, Most & Weih (2018) report a maximum TOV mass of $2.16^{0.17}_{0.15}\,\mathrm{M}_{\odot}$, and Shibata et al. (2017) provide an estimate for the maximum mass of 2.15–$2.25\,\mathrm{M}_{\odot}$. Recently, Shibata et al. (2019) revisited these constraints and found that the mass might only be constrained within $\lesssim 2.3\,\mathrm{M}_{\odot}$. All these constraints have been derived by assuming the formation of a BH after the merger of GW170817 and incorporating the measured chirp mass inferred from the GW analysis. Since our analysis was performed before the most recent constraints became available, we employ the maximum mass derived in Margalit & Metzger (2017); we also note that our results are only weakly sensitive to this choice; see the discussion below and the supplementary material for more details.

While overall many analyses of GW170817 and its EM signatures have been presented in the literature, we present here the first combined information from all three channels: GW170817, GRB170817A, and AT2017gfo. Our work uses more available knowledge than employed in any previous multimessenger analyses. In particular, our final posteriors describe the observed GW signature, the light-curve data of AT2017gfo, and explain the properties of GRB170817A. The flowchart in Fig. 1 highlights the interplay between the different observable signatures and presents the joint posteriors obtained on the tidal deformability $\tilde{\Lambda}$, the binary mass ratio q, and the maximum mass of a stable non-rotating neutron star M_{TOV}.

2 ANALYSIS

2.1 GW170817

We begin by analysing GW170817 (blue shaded region of Fig. 1) and use the publicly available 'low spin' posterior samples (https://dcc.ligo.org/LIGO-P1800370, Abbott et al. 2019b). As these sample use the sky localization obtained from EM observations, they already incorporate EM information. Under the assumption that the merging objects are two NSs described by the same EOS (Abbott et al. 2018; De et al. 2018), we can further restrict the posterior distribution. For this purpose, we use the posterior samples of Carson et al. (2019) where a same spectral EOS representation for both stars is employed. Finally, we discard those systems with viewing angles which are inconsistent with the ones obtained from the GRB afterglow by Troja et al. (2019).

2.2 AT2017gfo

In the second phase of our work, we analyse the light curves of AT2017gfo (red shaded region in Fig. 1). We fit the observational data (Abbott et al. 2017b; Smartt et al. 2017; Coughlin et al. 2018) with the two-component radiative transfer model of Kasen et al. (2017). The usage of multiple components, proposed prior to the discovery of GW170817 (Metzger & Fernández 2014), is motivated by different ejecta mechanisms contributing to the total r-process yields of BNS mergers. The first type of mass ejection are 'dynamical ejecta' generated during the merger process itself. Dynamical ejecta are typically characterized by a low-electron fraction when they are created by tidal torque, but the electron fraction can extend to higher values (and thus the lanthanide abundance be reduced) in the case of shock-driven ejecta. In addition to dynamical ejecta, disc winds driven by neutrino energy, magnetic fields, viscous evolution, and/or nuclear recombination (e.g. Kohri, Narayan & Piran 2005; Surman, McLaughlin & Hix 2006; Metzger, Piro & Quataert 2008; Dessart et al. 2009; Perego et al. 2014; Siegel, Ciolfi & Rezzolla 2014; Just et al. 2015) leads to a large quantity of ejecta, which in many cases exceeds that of the dynamical component. The ejecta components employed in our kilonova light-curve analysis are related to these different physical ejecta mechanisms: the first ejecta component is assumed to be proportional to dynamical ejecta, $m_{\mathrm{ej},1} = \alpha^{-1}\, m_{\mathrm{dyn}}$, while the second ejecta component arises from the disc wind and is assumed to be proportional to the mass of the remnant disc, $m_{\mathrm{ej},2} = \zeta\, m_{\mathrm{disc}}$. By fitting the observed light curves with the kilonova models (Kasen et al. 2017) within a GPR framework (Coughlin et al. 2018), we obtain for each component posterior distributions for the ejecta mass m_{ej}, the lanthanide mass fraction X_{lan} (related to the initial electron fraction), and the ejecta velocity v_{ej}.

The values of m_{ej}, X_{lan}, and v_{ej} obtained from our kilonova analysis are related to the properties of the binary and EOS using new phenomenological fits to NR simulations, which we briefly described below. First, we revisit the phenomenological fit presented in Radice et al. (2018c) between the disc mass and tidal deformability $\tilde{\Lambda}$ to correlate the disc mass, m_{disc}, to the properties of the merging binary. Simulations following the merger aftermath suggest that the disc mass is accumulated primarily through radial redistribution of matter in the post-merger remnant. Thus, the lifetime of the remnant prior to its collapse is related to its stability and found to strongly correlate with the disc mass (Radice et al. 2018a). We find that the lifetime in turn is governed to a large degree by the ratio of M/M_{thr}, where M is the total binary mass and

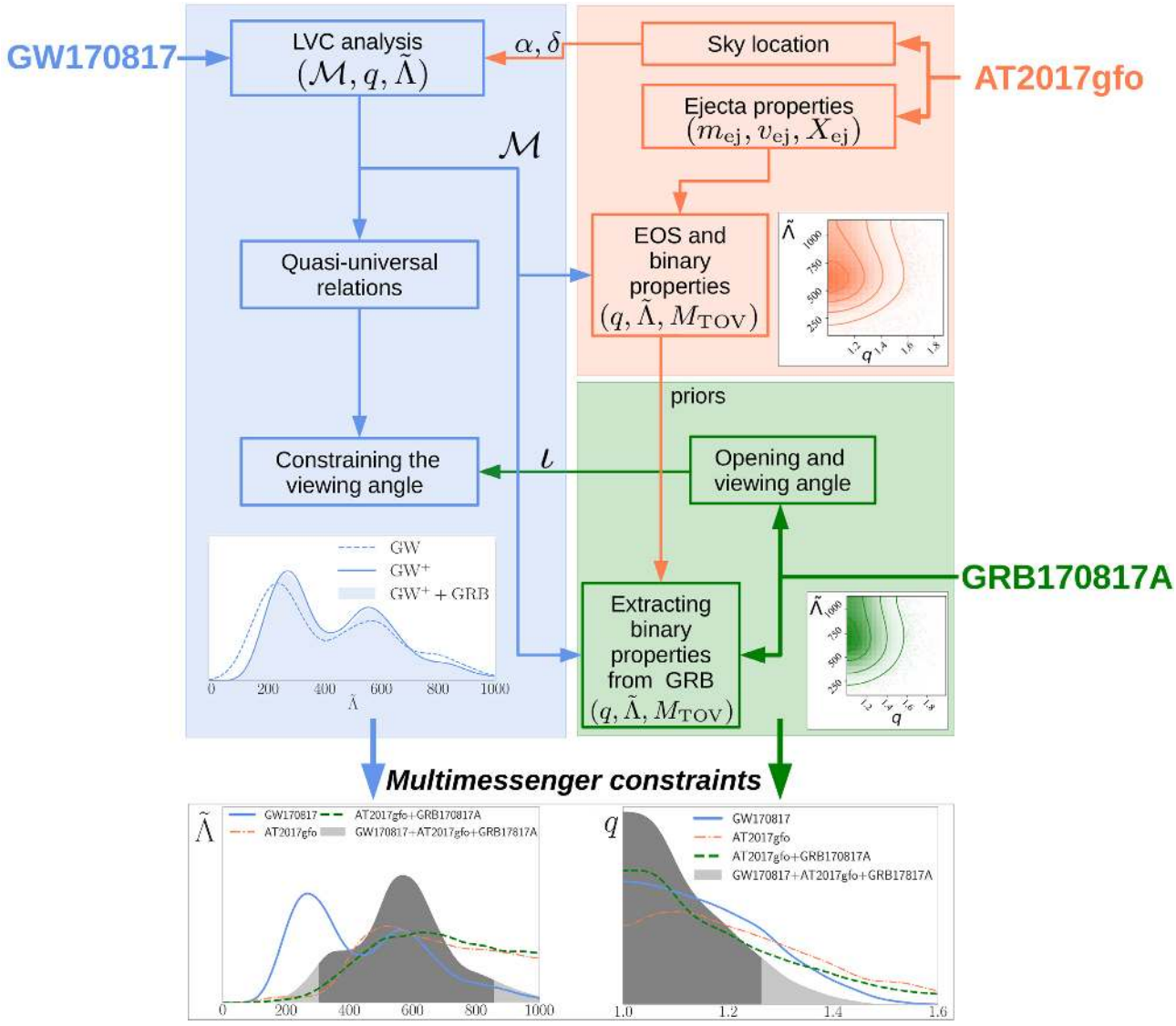

Figure 1. Flowchart of the analysis showcasing the analysis of GW170817, AT2017gfo, and GRB170817A. At the bottom of the panel, we show KDE posterior distributions of the tidal deformability (left-hand panel) and the mass ratio (right-hand panel). The final multimessenger result is shown as a shaded region, where the 90 per cent confidence interval is shaded darker. For the mass ratio, we assume a 90 per cent upper limit and for the tidal deformability we mark the 5th and 95th percentiles.

$M_{\rm thr}$ is the threshold mass (Bauswein, Baumgarte & Janka 2013) above which the merger results in prompt (dynamical time-scale) collapse to a black hole, which depends on the NS compactness and thus $\tilde{\Lambda}$. Therefore, $M/M_{\rm thr}$, rather than $\tilde{\Lambda}$ alone, provides a better measure of the stability of the post-merger remnant, and following the arguments above is expected to correlate with $m_{\rm disc}$.

Fig. 2 shows, based on the suite of NR simulations of Radice et al. (2018c), that there indeed exists a relatively tight correlation between the accretion disc mass and $M/M_{\rm thr}$. For our analysis, we will use

$$\log_{10}\left(m_{\rm disc}\left[M_{\rm tot}/M_{\rm thr}\right]\right) = \max\left(-3,\ a\left(1 + b\tanh\left[\frac{c - M_{\rm tot}/M_{\rm thr}}{d}\right]\right)\right), \quad (1)$$

with $M_{\rm thr}(M_{\rm TOV}, R_{1.6{\rm M}_\odot})$ as discussed in Bauswein et al. (2013) and the supplementary material, to describe the disc mass. The fitting parameters of equation (1) are $a = -31.335$, $b = -0.9760$, $c = 1.0474$, $d = 0.05957$.

Connecting the NS radius to the chirp mass and tidal deformability, $R = \mathcal{M}(\tilde{\Lambda}/a)^{1/6}$ (De et al. 2018), we conclude that the disc mass (and thus the disc wind ejecta) is a function of the tidal deformability, total binary mass, and the maximum TOV mass, $M_{\rm TOV}$. Therefore, both information, those on the densest portion of the EOS, which controls $M_{\rm TOV}$, and those from lower densities, as encoded in $\tilde{\Lambda}$ or $R_{1.6\,{\rm M}_\odot}$, play a role in controlling the disc mass and kilonova properties. The inclusion of these parameters and slight changes in the functional form of the phenomenological relation decrease the average fractional errors by more than a factor of three relative to previous disc mass estimates based on $\tilde{\Lambda}$ alone (Radice et al. 2018a), thus reducing uncertainties and errors on the EOS constraints obtained from kilonova observations.

Another key ingredient in our analysis is the role of the dynamical ejecta as the first kilonova ejecta component. Based on a suite of

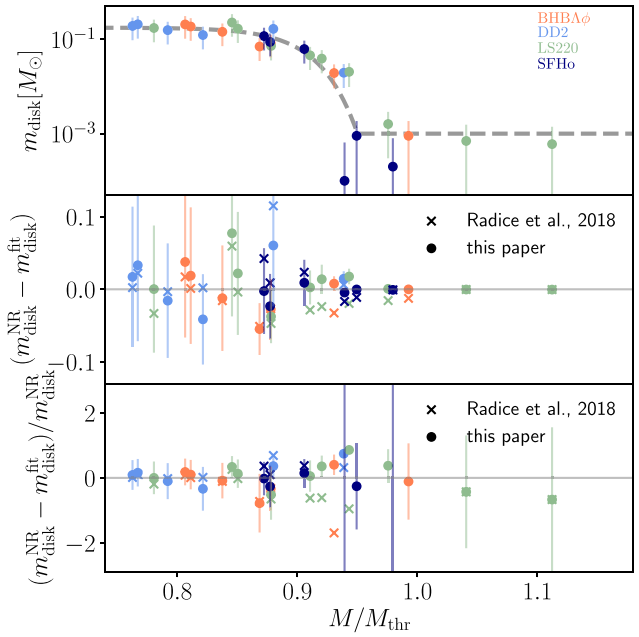

Figure 2. Disc masses as a function of the ratio between the total mass and the threshold mass for prompt BH formation. The disc mass estimates are obtained from the NR simulations presented in Radice et al. (2018c). The error bars refer to $(0.5 m_{\rm disc} + 5 \times 10^{-4}\,{\rm M}_\odot)$ as stated in the original work of Radice et al. (2018c). The threshold mass for prompt BH formation is computed following Bauswein et al. (2013). We present our best fit, equation (1), in the top panel and show the absolute and fractional errors of the phenomenological fit in the middle and bottom panel. We compare our results with the original version of the fit presented in Radice et al. (2018c).

NR simulations obtained by different groups and codes, Dietrich & Ujevic (2017) derived the first phenomenological fit for the dynamical ejecta for BNS systems. This fit (in its original or upgraded version) has been employed in a number of studies, including the analysis of GW170817 (Abbott et al. 2017d; Coughlin et al. 2018), and they have been updated in Coughlin et al. (2018) and Radice et al. (2018c). Here, we present a further upgrade which incorporates the new NR data set of Radice et al. (2018c) and uses the fitting function of Coughlin et al. (2018) (which fits $\log_{10} m_{\rm dyn}$ instead of $m_{\rm dyn}$). The extended data set contains a total of 259 NR simulations. The final fitting function is

$$\log_{10} m^{\rm fit}_{\rm dyn} = \left[a \frac{(1-2\,C_1)M_1}{C_1} + b\,M_2 \left(\frac{M_1}{M_2}\right)^n + \frac{d}{2}\right] + [1 \leftrightarrow 2], \quad (2)$$

with $a = -0.0719$, $b = 0.2116$, $d = -2.42$, and $n = -2.905$ and $C_{1,2}$ denoting the compactnesses of the individual stars, a more detailed discussion can be found in the supplementary material.

A final ingredient in relating observational data to the binary parameters are phenomenological fits for the BH mass and spin. One finds that with an increasing total mass M, the final black hole mass and angular momentum increase almost linearly. For unequal mass mergers, $M_{\rm BH}$ and $\chi_{\rm BH}$ decrease with M. Considering the imprint of the EOS, we find that for larger values of $\tilde{\Lambda}$, the final black hole mass decreases, which follows from the observation that the disc mass increases with $\tilde{\Lambda}$. We finally obtain:

$$M_{\rm BH} = a \left(\frac{\nu}{0.25}\right)^2 \left(M + b\,\frac{\tilde{\Lambda}}{400}\right) \quad (3)$$

with $a = 0.980$ and $b = -0.093$ and

$$\chi_{\rm BH} = \tanh\left[a\nu^2(M + b\,\tilde{\Lambda}) + c\right] \quad (4)$$

with $a = 0.537$, $b = -0.185$, and $c = -0.514$; further details are given in the supplementary material.

In addition to using these fits, we use the results of Margalit & Metzger (2017), who derive a 90 per cent upper limit on the mass of a non-rotating NS of $2.17\,{\rm M}_\odot$ based on energetic considerations from the GRB and kilonova which rule out a long-lived supramassive NS remnant, to place a prior on $M_{\rm TOV}$ between 2 and $2.17\,{\rm M}_\odot$. Combining these phenomenological relations with the light-curve data, our analysis strongly favours equal or nearly equal-mass systems and $\tilde{\Lambda} \geq 400$ (see supplementary material). We conclude that roughly 20 per cent of the first ejecta component is associated with dynamical ejecta, while about 20 per cent of the disc mass must be ejected in winds to account for the second ejecta component. The latter agrees with the results of long-term general relativistic magnetohydrodynamical simulations of the post-merger accretion disc (e.g. Siegel & Metzger 2017). If we do not enforce constraints on $M_{\rm TOV}$, we obtain similar constraints in the binary parameters but with allowed values $M_{\rm TOV} = 2.28^{+0.34}_{-0.33}\,{\rm M}_\odot$. This is broadly consistent with the results presented in Margalit & Metzger (2017); Rezzolla, Most & Weih (2018); Ruiz, Shapiro & Tsokaros (2018); Shibata et al. (2019) and provides a new and independent measurement of the maximum TOV mass, which will become more accurate with future multimessenger events. Full posteriors for the analysis without enforced constraints on $M_{\rm TOV}$ can be found in the supplementary material.

2.3 GRB170817A

Our third and final result uses Bayesian parameter estimation of GRB170817A directly (green shaded region in Fig. 1). We assume that the GRB jet is powered by the accretion of matter from the debris disc on to the BH (Eichler et al. 1989; Paczynski 1991; Meszaros & Rees 1992; Narayan, Paczynski & Piran 1992) and that the jet energy is proportional to the disc mass. Accounting for the loss of disc mass to winds, we connect our estimates of the disc wind ejecta from the analysis of AT2017gfo to the following GRB parameter estimation analysis. In order to assess the robustness of our conclusions, and to evaluate potential systematic uncertainties, we show results for three different fits to the GRB afterglow: Troja et al. (2019), Wu & MacFadyen (2018), and Wang et al. (2019). While the analyses of Troja et al. (2019) and Wu & MacFadyen (2018) differ on the energy of the GRB, the use of either one further constrains the value of $\tilde{\Lambda}$ and the binary mass ratio, shifting both to slightly higher values than obtained through the analysis of AT2017gfo alone.

3 MULTIMESSENGER CONSTRAINTS

To obtain the final constraints on the EOS and binary properties, we combine the posteriors obtained from GW170817 and AT2017gfo+GRB170817A. The analysis of AT2017gfo and GRB170817A are highly correlated, as both use the same phenomenological description for the disc mass and the AT2017gfo posteriors are employed as priors for the GRB analysis. However, we assume the parameter estimation results from the GW and EM analysis for $\tilde{\Lambda}$ and q are independent from one another. Thus, the final multimessenger probability density function is given by:

$$P_{\rm MMA} = P_{\rm GW170817} \times P_{\rm AT2017gfo+GRB10817A}. \quad (5)$$

Table 1. Final multimessenger constraints on the EOS and the binary properties of GW170817. The radius constraint has to be assigned with an additional 0.2 km uncertainty due to the employed quasi-universal relations of De et al. (2018).

Parameter	90 per cent confidence interval
M	$[2.722, 2.751]\,\mathrm{M}_\odot$
q	[1.00, 1.27]
$\tilde{\Lambda}$	[302, 860]
R	[11.1, 13.7] km

In principle, there are also contributions from the priors in P_{MMA}, but because they are flat over the bounds considered, it is valid. We summarize our constraints on the binary parameters and EOS in Table 1. The final constraints on the tidal deformability and the mass ratio are shown at the bottom of Fig. 1, where we use the GRB model of Troja et al. (2019) (similar constraints are obtained with the other GRB models). According to our analysis, the 90 per cent confidence interval for the tidal deformability is $\tilde{\Lambda} \in (302, 860)$. The distribution has its 50 per cent percentile at $\tilde{\Lambda} \sim 569$. Relating the measured $\tilde{\Lambda}$ confidence interval to the NS radius (De et al. 2018), we obtain a constraint on the NS radius of $R \in (11.3, 13.5)$ km [with a ± 0.2 km uncertainty of the quasi-universal relation (De et al. 2018; Radice & Dai 2019) connecting $\tilde{\Lambda}$ and R]. This result is in good agreement with that recently obtained by the multimessenger analysis presented in Radice & Dai (2019). Considering the constraint on the mass ratio, we find that $q \leq 1.27$ at 90 per cent confidence. Combining this with the measured chirp mass, the total binary mass $M = \mathcal{M}\left(\frac{(1+q)^2}{q}\right)^{3/5}$ lies in the range $M \in [2.722, 2.751]\,\mathrm{M}_\odot$. The radius constraint, together with the constraint on the maximum TOV-mass, can be used to rule out or favour a number of proposed NS EOSs, as illustrated in Fig. 3.

We note that there are a number of potential systematic uncertainties in the presented analysis, which we, however, tried to incorporate and minimize. In general, we have assumed that the kilonova and GRB models are sufficient to generate quantitative conclusions. To be robust against uncertainties, we have employed large systematic error bars for the kilonova analysis as described in Coughlin et al. (2018). In addition, the merger simulations and thereby the determination of ejecta and disc masses may still have large uncertainties because of limited resolution and missing physics, see e.g. Kiuchi et al. (2019). These uncertainties and the specific simulations used can quantitatively change the results; for example Kiuchi et al. (2019) showed, using a different simulation set, that the possibility that GW170817 was a relatively high mass ratio system argues for an even lower bound, $\tilde{\Lambda} \geq 242$, than presented here. The α and ξ variables encode some of the uncertainty associated with this fact, as they just assume that the simulations are broadly correct up to a scale factor, but they will be incapable of encoding large changes in this result in the case of non-linear effects. In addition, while the employed GRB models are relatively simplistic, we have included three different GRB analyses, showing that they, in general, produce consistent results.

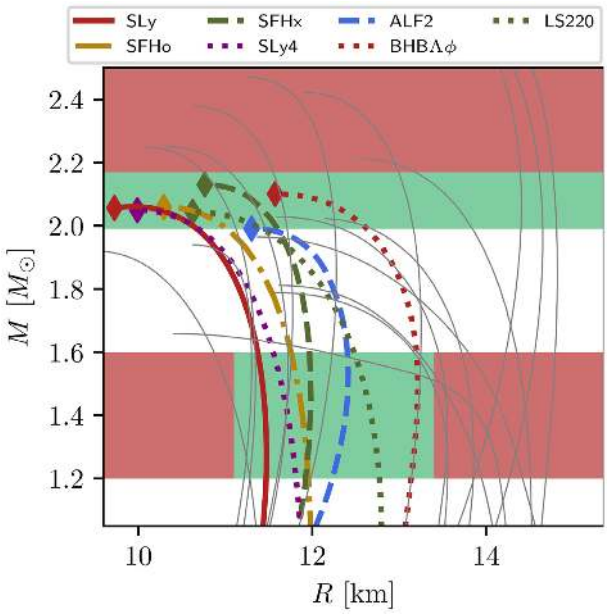

Figure 3. EOS overview including the known constraints on the maximum TOV mass and the NS radius. Realistic EOSs need to fall within the green shaded regions and are outside the 90 per cent confidence intervals in the red areas. We only show a sample of a larger number of existing EOSs and only label the EOSs consistent with our constraints.

ACKNOWLEDGEMENTS

We thank Zoheyr Doctor, Michael Pürrer, and David Radice for helpful discussions and comments on the manuscript. We are particularly thankful to Zack Carson, Katerina Chatziioannou, Carl-Johan Haster, Kent Yagi, Nicolas Yunes for providing us their posterior samples analysing GW170817 under the assumption of a common EOS (Carson et al. 2019). MWC is supported by the David and Ellen Lee Postdoctoral Fellowship at the California Institute of Technology. TD acknowledges support by the European Union's Horizon 2020 research and innovation program under grant agreement No 749145, BNSmergers. BDM is supported in part by NASA through the Astrophysics Theory Program (grant # NNX16AB30G). BM is supported by NASA through the NASA Hubble Fellowship grant #HST-HF2-51412.001-A awarded by the Space Telescope Science Institute, which is operated by the Association of Universities for Research in Astronomy, Inc., for NASA, under contract NAS5-26555.

REFERENCES

Abbott B. P. et al., 2017a, Phys. Rev. Lett., 119, 161101
Abbott B. P. et al., 2017b, ApJ, 848, L12
Abbott B. P. et al., 2017c, ApJ, 848, L13
Abbott B. P. et al., 2017d, ApJ, 850, L39
Abbott B. P. et al., 2018, Phys. Rev. Lett., 121, 161101
Abbott B. P. et al., 2019a, Phys. Rev. X, 9, 011001
Abbott B. P. et al., 2018b, Phys. Rev. X, 9, 031040
Arcavi I. et al., 2017, Nature, 551, 64
Bauswein A., Baumgarte T. W., Janka H.-T., 2013, Phys. Rev. Lett., 111, 131101
Bauswein A., Just O., Janka H.-T., Stergioulas N., 2017, ApJ, 850, L34
Carson Z., Chatziioannou K., Haster C.-J., Yagi K., Yunes N., 2019, Phys. Rev. D, 99, 083016
Coughlin M. W. et al., 2018, MNRAS, 480, 3871
Coulter D. A. et al., 2017, Science, 358, 1556
Dai L., Venumadhav T., Zackay B., 2018, preprint (arXiv:1806.08793)
De S., Finstad D., Lattimer J. M., Brown D. A., Berger E., Biwer C. M., 2018, Phys. Rev. Lett., 121, 091102
Dessart L., Ott C. D., Burrows A., Rosswog S., Livne E., 2009, ApJ, 690, 1681

Dietrich T., Ujevic M., 2017, Class. Quantum Gravity, 34, 105014
Doctor Z., Farr B., Holz D. E., Pürrer M., 2017, Phys. Rev., D96, 123011
Dudi R., Pannarale F., Dietrich T., Hannam M., Bernuzzi S., Ohme F., Brügmann B., 2018, Phys. Rev. D, 98, 084061
Eichler D., Livio M., Piran T., Schramm D. N., 1989, Nature, 340, 126
Finstad D., De S., Brown D. A., Berger E., Biwer C. M., 2018, ApJ, 860, L2
Just O., Bauswein A., Pulpillo R. A., Goriely S., Janka H. T., 2015, MNRAS, 448, 541
Kasen D., Metzger B., Barnes J., Quataert E., Ramirez-Ruiz E., 2017, Nature, 551, 80
Kiuchi K., Kyutoku K., Shibata M., Taniguchi K., 2019, ApJ, 876, L31
Kohri K., Narayan R., Piran T., 2005, ApJ, 629, 341
Lipunov V. M. et al., 2017, ApJ, 850, L1
Margalit B., Metzger B. D., 2017, ApJ, 850, L19
Meszaros P., Rees M. J., 1992, ApJ, 397, 570
Metzger B. D., Fernández R., 2014, MNRAS, 441, 3444
Metzger B. D., Piro A. L., Quataert E., 2008, MNRAS, 390, 781
Narayan R., Paczynski B., Piran T., 1992, ApJ, 395, L83
Paczynski B., 1991, Acta Astron., 41, 257
Perego A., Rosswog S., Cabezón R. M., Korobkin O., Käppeli R., Arcones A., Liebendörfer M., 2014, MNRAS, 443, 3134
Pürrer M., 2014, Class. Quantum Gravity, 31, 195010
Radice D., Dai L., 2019, Eur. Phys. J. A, 55, 50
Radice D., Perego A., Bernuzzi S., Zhang B., 2018a, MNRAS, 481, 3670
Radice D., Perego A., Zappa F., Bernuzzi S., 2018b, ApJ, 852, L29
Radice D., Perego A., Hotokezaka K., Fromm S. A., Bernuzzi S., Roberts L. F., 2018c, ApJ, 869, 130
Rezzolla L., Most E. R., Weih L. R., 2018, ApJ, 852, L25
Ruiz M., Shapiro S. L., Tsokaros A., 2018, Phys. Rev., D97, 021501
Samajdar A., Dietrich T., 2018, Phys. Rev. D, 98, 124030
Shibata M., Fujibayashi S., Hotokezaka K., Kiuchi K., Kyutoku K., Sekiguchi Y., Tanaka M., 2017, Phys. Rev., D96, 123012
Shibata M., Zhou E., Kiuchi K., Fujibayashi S., 2019, Phys. Rev. D, 100, 023015
Siegel D. M., Metzger B. D., 2017, Phys. Rev. Lett., 119, 231102
Siegel D. M., Ciolfi R., Rezzolla L., 2014, ApJ, 785, L6
Smartt S. J. et al., 2017, Nature, 551, 75
Soares-Santos M. et al., 2017, ApJ, 848, L16
Surman R., McLaughlin G. C., Hix W. R., 2006, ApJ, 643, 1057
Tanvir N. R. et al., 2017, ApJ, 848, L27
Troja E. et al., 2019, MNRAS, preprint (arXiv:1808.06617)
Valenti S. et al., 2017, ApJ, 848, L24
Wang Y.-Z. et al. 2019, ApJ, 877, 2
Wu Y., MacFadyen A., 2018, ApJ, 869, 55

SUPPORTING INFORMATION

Supplementary data are available at *MNRASL* online.

Multimessenger Bayesian parameter inference of a binary neutron star merger – Letter Supplement.zip

Please note: Oxford University Press is not responsible for the content or functionality of any supporting materials supplied by the authors. Any queries (other than missing material) should be directed to the corresponding author for the article.

This paper has been typeset from a TEX/LATEX file prepared by the author.